

Article

Characterisation of Bottom Ashes from Non-Woody Biomass Combustion for Application as Sustainable Supplementary Cementitious Material

Rafiandy Dwi Putra ^{1,*}, Hossein Beidaghy Dizaji ¹, Driпти Kulshresth ¹, Thomas Zeng ¹ , Steffen Overmann ²  and Anya Vollpracht ²

¹ DBFZ Deutsches Biomasseforschungszentrum Gemeinnützige GmbH, 04347 Leipzig, Germany; beidaghy88@gmail.com (H.B.D.); driпти26@gmail.com (D.K.); thomas.zeng@dbfz.de (T.Z.)

² Institute of Building Materials Research—Construction Materials, RWTH Aachen University, 52062 Aachen, Germany; overmann@ibac.rwth-aachen.de (S.O.); vollpracht@ibac.rwth-aachen.de (A.V.)

* Correspondence: rafiandy.dwi.putra@dbfz.de

Abstract: Cement production is an energy- and resource-intensive industry accounting for approximately 7% of global carbon dioxide emissions. Therefore, a key decarbonisation option for the cement industry is to substitute the clinker with so-called supplementary cementitious materials (SCMs). Due to its properties and availability, the bottom ash from the biomass combustion process could be suitable as an SCM. Several agricultural residues were collected and analysed. The materials were applied for ashing experiments in a lab-scale muffle furnace, which was operated at different temperatures. The chemical, physical, and mineralogical characterisation of the ashes produced was carried out. In addition, the reactivity of the cementitious paste made from the ashes was measured through lab-scale experiments. The influence of the different ashing temperatures and the additive mixing on the properties of the ashes and cementitious paste was analysed. The results show that the spelt husk ash is the most promising biomass ash, with its high silica content and high pozzolanic reactivity. The bound water of the cementitious paste made from spelt husk ash reaches 7.3 g/100 g paste at 700 °C but decreases to 2.5 g/100 g paste at 900 °C due to the formation of a crystalline structure. Nevertheless, the addition of kaolin to the spelt husk can maintain the reactivity of the spelt husk ash produced at high ashing temperatures by stabilising the amorphous structure in the ash.

Keywords: biomass; agricultural residues; ash; combustion; supplementary cementitious material



Citation: Putra, R.D.; Dizaji, H.B.; Kulshresth, D.; Zeng, T.; Overmann, S.; Vollpracht, A. Characterisation of Bottom Ashes from Non-Woody Biomass Combustion for Application as Sustainable Supplementary Cementitious Material. *Energies* **2024**, *17*, 468. <https://doi.org/10.3390/en17020468>

Academic Editors: Solange I. Mussatto and David Baxter

Received: 22 December 2023

Revised: 10 January 2024

Accepted: 15 January 2024

Published: 18 January 2024



Copyright: © 2024 by the authors. Licensee MDPI, Basel, Switzerland. This article is an open access article distributed under the terms and conditions of the Creative Commons Attribution (CC BY) license (<https://creativecommons.org/licenses/by/4.0/>).

1. Introduction

Concrete is an essential material in the construction sector, and it is one of the most demanded products in the world [1]. The main conventional binder used in concrete is Portland cement, which has a significant impact on the environmental footprint of concrete production [2,3]. Portland cement production is an energy- and resource-intensive industry that still relies heavily on fossil fuels, such as lignite and hard coal. The main part of carbon dioxide release during clinker production comes not only from the combustion of fossil fuel but from the thermal decomposition of limestone. Consequently, the cement industry is accountable for approximately 7% of global carbon dioxide emissions [4]. This represents a major challenge to achieving the Paris Agreement's goal of limiting global warming to below 2 °C [5].

Efforts to achieve a more sustainable cement production industry have been gaining interest in recent years. In addition to potential solutions, such as carbon capture and storage, alternative fuels, and energy efficiency, it is becoming more apparent that one of the economically viable options to abate the carbon dioxide emissions from cement production is to partially substitute clinker with sustainable supplementary cementitious materials (SCMs) [6]. SCMs are pozzolanic or hydraulic materials that typically contain

silicate, aluminosilicate, or calcium aluminosilicate that are obtained from less carbon-intensive processes. Commonly employed SCMs are usually derived from industrial waste streams, such as coal fly ash and blast-furnace slag [7]. However, especially in the case of coal fly ash, the supply chain will not be sustainable in the future. Due to stricter environmental constraints leading to the shutdown of coal-fired power plants in some European countries, the cement industry will face a more limited availability of these coal-based SCMs.

On the other hand, the utilisation of biomass in the energy sector is growing. Biomass energy accounts for about 60% of the total renewable energy supply in the EU, which is dominated by woody biomass [8]. Biomass combustion produces two types of biomass ash as by-products: coarse bottom ash, which consists of inorganic constituents and unburnt carbon, and fine fly ash, which is collected in filters and is typically rich in potassium, chlorine, and sulphur [9]. In grate combustion, bottom ash accounts for approximately 60–90% of the total biomass ash produced [10].

The use of biomass ash as SCMs in the cement industry is considered a potential valorisation route of biomass ash [11,12]. Several studies have investigated the application of fly ash from woody biomass combustion as partial substitutions of Portland cement [13–18]. For instance, Fořt et al. suggest biomass fly ash can substitute up to 20 wt.% of cement binder without significantly reducing the mechanical strength of the cement mixture [14]. On the other hand, only a few studies have focused on the use of biomass ash as SCMs, including, in particular, from ash-rich, non-woody agricultural residues. Only rice husk ash has received some attention as an SCM, particularly due to its high silica content [19–21]. However, due to the low regional availability of rice husk in the EU, the evaluation of other available non-woody biogenic residues becomes more important from a supply chain perspective.

Biomass ash transformation is a complex process, particularly with regards to the challenging fuel ash compositions of non-woody biomass fuels compared to sawdust [22]. Biomass ash, especially non-woody biomass, often contains a higher share of elements, such as potassium, chlorine, and sulphur, that can cause operational problems during combustion [23]. To mitigate ash-related problems, non-woody biomass fuels are in some cases blended with other biomasses or additives, such as kaolin [23,24]. Kaolin is known as an aluminium-based additive that can hinder the slagging tendency during thermochemical processes of biomass [25–27]. During combustion, kaolin reacts with critical ash-forming elements, like K and Na, to form high-melting crystalline compounds, like kalsilite (KAlSiO_4) and leucite (KAlSi_2O_6), thus preventing slag formation [24,28]. Although the addition of kaolin has been proven to reduce slagging behaviour during the combustion of non-woody biomass, its effect on the pozzolanic properties of biomass ash has not been widely explored, particularly with regards to the tendency of the formation of crystalline structures.

In this study, the chemical, physical, and mineralogical properties of bottom ashes from the combustion of highly available non-woody biomass are investigated with regards to their valorisation as SCMs at different ashing temperatures. Furthermore, the pozzolanic reactivity of these ashes in cementitious paste is measured through laboratory-scale experiments. Finally, the ability of kaolin as an additive to improve the characteristics and reactivity of the biomass ashes is investigated.

2. Materials and Methods

2.1. Biomass Fuel Selection and Preparation

The biomass fuels used in this study were selected based on their characteristics and availability in Germany. According to Eurostat, wheat and spelt are the most produced cereals in Germany, with an annual production of 22 million tonnes in 2020 [29]. Therefore, spelt husk was selected. Moreover, oat husk and hay are also included in this study due to their potentially high ash content (AC) and seasonal availability. Finally, digestate and foliage were selected due to their promising properties as alternative sustainable fuels. Rice husk was selected as a reference, as it has been proposed as an alternative SCM from

previous studies [21,30,31]. Thus, the biomasses used in this study are as follows: spelt husk (SH), oat husk (OH), hay (H), digestate (D), washed foliage (F), and rice husk (RH) as a reference. In the case of SH, 1 wt.% of kaolin was added to produce additivated spelt husk (ASH) pellets. The kaolin was purchased from Surmin-Kaolin S.A. The chemical composition of the kaolin used as an additive in this research is presented in Table A1.

The scheme of the biomass fuel preparation and the ash production (Section 2.2) is illustrated in Figure 1. First, the biomass was crushed to a particle size of 4 mm using a hammer mill (CHM230/200, NETZSCH, Selb, Germany). The biomass fuel was then conditioned and mixed with water using a mixer (MSX550, Process Technology GmbH, Walldürn, Germany) to increase the moisture content of the fuel to 20 wt.%. To produce ASH, kaolin was added to the conditioning water. Once the biomass reached its required moisture, it was pelletised into pellets with a diameter of 6 mm using a commercial ring dye press (Maxima 360–403 K, Salmatec GmbH, Gödenstorf, Germany). Prior to the ashing process, the pellet batches, each approximately 50 kg, were homogenised using a mixer and screened to reduce fine fractions (<3.15 mm).

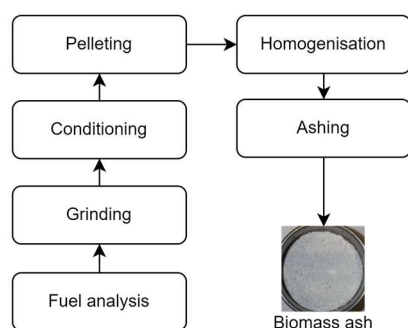


Figure 1. Biomass ash production method.

2.2. Ashing Method

The ashing of the biomass pellets was carried out in a muffle furnace (1185H66EA, Nabertherm GmbH, Lilienthal, Germany) under an air atmosphere. The biomass pellets were heated from room temperature to the final temperature at a heating rate of 10 K/min. The final ashing temperatures of 700 °C, 800 °C, and 900 °C were selected based on previous studies that indicated a change in the structural characteristics and composition of the biomass ash in the range of 700 °C and 900 °C [32–34]. Higher ashing temperatures are not considered as they may induce slag formation and produce ashes with a high content of crystalline phases [35,36]. The final ashing temperature was kept constant for 2 h. In total, 400 g of biomass pellets was used for each ashing experiment. Each ashing experiment was repeated several times to produce a sufficient amount of biomass ash (at least 200 g) for the subsequent characterisation and analysis (Section 2.3).

2.3. Biomass Ash Characterisation

The AC of the biomass fuel was analysed at 550 °C according to the standard of AC determination in solid biofuels [37]. To analyse the chemical composition of the biomass fuel and ash, elemental analyses were performed using the inductively coupled plasma optical emission spectroscopy (ICP-OES) method after hydrofluoric digestion according to DIN EN ISO 16967:2015-07 [38]. The loss on ignition (LOI) of biomass ashes was determined according to DIN EN 15935:2021-10 [39].

For the mineralogical characterisation, the samples were ground by hand with an agate mortar until a grain size of <63 µm. The mineralogical composition was determined using an X-ray diffractometer (XRD) Panalytical X'Pert Pro with an X'Celerator detector. Data were acquired in the range of 5 to 70 °2θ with a step size of 0.0167 °2θ and a total measurement time of 2 h. Rietveld refinement was performed to determine the quantitative composition of the samples using the software Panalytical Highscore Plus 4.8 with ICSD database version 1.5 from FIZ Karlsruhe. An internal rutile standard was used to quantify

the amorphous content. In addition, the textural properties of the ashes were characterised using the Brunauer–Emmet–Teller (BET) specific surface area (SSA). The BET method is the most widely used tool for measuring the surface area of porous material [40]. The textural analysis was performed using the autosorb apparatus (iQ-MP/XR, Quantachrome Instruments, Boynton Beach, FL, USA). Nitrogen was used as the adsorptive gas at 77 K, with a standard molecular cross section of 0.162 nm² [41]. The BET specific surface area was determined in the pressure range of $p/p_0 = 0.05\text{--}0.3$, and prior to the gas sorption experiments, the samples were degassed and activated under ultrahigh vacuum for 12 h at 250 °C [42,43]. The pH of the ash samples was measured according to the standard soil pH measurement (ASTM D4972) [44].

2.4. Pozzolanic Reactivity Test

The reactivity of the cementitious paste was determined according to the measuring bound water and the cumulative heat of hydration during the curing process, as described in ASTM C1897-20 [45]. This method was developed as a new, rapid, relevant, and reliable (R3) method to evaluate the pozzolanic reactivity of cementitious pastes using simple instruments, which are often available in scientific laboratories [46]. Round-robin tests were conducted to validate the results of both methods [47]. Both test methods have been shown to correlate well with the benchmark 28 days relative strength.

According to ASTM C1897-20, the ash was mixed with Ca(OH)₂ and CaCO₃ in a ratio of 2:6:1, respectively. After tempering the dry mix at 40 °C, the potassium solution tempered at the same temperature was added to the solids and mixed with a high-shear blender to form a cementitious paste. The potassium solution was a mixture of 4 g of KOH and 20 g of K₂SO₄ dissolved in 1 L of reagent water. The mass ratio of the dry mixture to the potassium solution was 1:1.2.

2.4.1. Isothermal Calorimetry

Isothermal calorimetry is used to determine the heat released during the reaction process, which gives an indication of the reactivity of a particular sample. Heat release was measured using isothermal calorimetry (TAM Air, TA instruments, New Castle, DE, USA). Each 15 g of the samples was weighted in two sample vessels for duplicate determination. Tap water was used as a reference. The samples were immediately placed in the calorimeter, and the heat of the reaction was recorded for 7 days. For evaluation, the first 75 min were cut off according to the ASTM C1897-20 [45].

2.4.2. Bound Water Measurement

The chemical reactivity of the paste was determined by measuring the chemically bound water in the paste [44]. For the bound water measurement, the paste had to undergo a curing process. Paste samples were kept in airtight containers in a drying cabinet (FED 240, BINDER GmbH, Tuttlingen, Germany) at 40 °C to accelerate the reaction rate of slow-reacting SCMs. After seven days, the hardened paste was ground to a particle size of less than 2 mm. To remove unbound water, the pastes were transferred to petri dishes before being returned to the drying rack for a further 24 h at the same temperature.

To measure the chemically bound water, the dried paste was heated in a muffle furnace at 350 °C for 2 h. The bound water content of the paste was calculated as follows:

$$BW_{paste} = \frac{(w_i - w_f)}{(w_i - w_c)} \times 100 \% \quad (1)$$

where:

BW_{paste} : chemically bound water content of the paste;

w_i : total mass of the paste sample and crucible before heating;

w_f : total mass of the paste sample and crucible after heating;

w_c : mass of the crucible.

The bound water content of the paste must be corrected with the original chemically bound water of the SCM, which was calculated as follows

$$BW_{SCM} = \frac{(w_{i,SCM} - w_{f,SCM})}{(w_{i,SCM} - w_c)} \times 100 \% \quad (2)$$

where:

BW_{SCM} : chemically bound water content of the SCM;

$w_{i,SCM}$: total mass of the SCM sample and crucible before heating;

$w_{f,SCM}$: total mass of the SCM sample and crucible after heating;

w_c : mass of the crucible.

The corrected bound water of the paste was subsequently calculated as follows:

$$BW_{corr.} = BW_{paste} - (0.101 \times BW_{SCM}) \quad (3)$$

wherein the coefficient 0.101 is the mass fraction of the SCM in the paste.

2.5. Thermodynamic Equilibrium Calculations

Thermodynamic equilibrium calculations are a powerful method for modeling and simulating the transformation of any biomass fuel constituents during thermochemical conversion processes. The calculation is based on the minimisation of the total Gibbs energy of all chemical reactions that can occur in the system. It is an iterative process that considers each possible chemical reaction based on the selected database. In this study, this method was used to predict the slagging behaviour and the transformation of the solid phases in biomass ashes during the ashing process. The mineral phases of the ash were compared quantitatively with results from the XRD analysis (Section 2.3). FactSage 8.2 was used to perform the calculations. This software was chosen because of its extensive databases of molten salts and slags, and because of the high similarity between the results of this simulation and the quantitative XRD phase analysis in our previous publications [35].

The organic and major ash-forming elements (C, H, O, N, Al, Ca, K, Mg, P, S, Si, and Cl) of the biomass fuel were used as simulation inputs. In addition, atmospheric air (21 vol% O₂, 79 vol% N₂) was added as an additional input. The excess air ratio was set to simulate a rich combustion with excess air ($\lambda = 1.15$), and the ash transformation process pressure was set to 1 atm. The temperature was set between 700 °C and 900 °C and was monitored by 50 K intervals. The transitions during the phase transformation were also observed.

The 'Equilib' module of the FactSage 8.2 software was used to simulate the thermodynamic calculation. The databases FactPS, FToxid, and FTsalt provided the thermodynamic data of the pure substances, oxides, and salts, respectively. According to Lindberg et al. [48], the FToxid database provides the most comprehensive data on oxides and silicates in solid and liquid forms. The data of the solution phases were obtained from the FToxid-SlagB database. The SlagB database identifies liquid solutions of various oxides that can dissolve sulphur as sulphates. Although sulphates, such as K₂SO₄, are commonly found in biomass ash [49], SlagB has never been optimised for the K₂O–CaO–SiO₂ system. Therefore, SlagA was chosen for this calculation. In the case of similar chemical species in these databases, priority was given in the order of FToxid, FTsalts, and FactPS, and duplicates were suppressed.

3. Results and Discussion

3.1. Pre-Evaluation Based on Fuel Ash Composition

The evaluation criteria developed for the preliminary assessment of the potential of the biomass ash are summarised in Table 1. The criteria have been adopted from the standard requirement for the use of silicate fly ash in concrete [50]. SiO₂, Al₂O₃, and Fe₂O₃ are the pozzolanic oxides that may react in the presence of calcium to bound hydrate components [51]. A high content of these elements is beneficial for the properties of SCM

if they are in soluble states. Several species, such as MgO, Na₂O, P₂O₅, SO₃, and Cl, are limited to a certain value as they can impair concrete quality. For instance, a high Cl content increases the risk of corrosion [52]. In addition to the limit values listed in DIN EN 450-1, the potassium content is also chosen as an evaluation parameter, as it often correlates with the risk of slagging [52] and the risk of high particulate matter emissions during biomass combustion.

Table 1. Selection criteria for pre-evaluation. Adapted from DIN EN 450-1 [50] (db: dry basis).

Parameter	Value (wt.% db)
AC	as high as possible
K ₂ O	as low as possible
MgO	≤4
Na ₂ O	≤5
P ₂ O ₅	≤5
SiO ₂ + Al ₂ O ₃ + Fe ₂ O ₃	≥70
SiO ₂	as high as possible
SO ₃	≤3
Cl	≤0.10

The results of the evaluation with respect to the selection criteria (Table 1) are presented in Table 2. The full results of the chemical analysis of the fuels are presented in Table A2. Based on the results, several biomasses did not meet the selection criteria. OH and H were neglected due to the low AC (OH: 5.4 wt.% db, H: 5.6 wt.% db) and high potassium content (OH: 15.0 wt.% db, H: 45.3 wt.% db). Potassium is one of the main constituents that can induce slagging [52]. In addition, D was also excluded from further analyses due to its high phosphorus content, which reached 21.6 wt.% db. As concluded by Al Pang et al., phosphorus content in the range of 10 wt.% db and 50 wt.% db may interfere with the setting time of the cement and thus induce micro-cracks [53].

Table 2. Fuel ash composition (in wt.% db) of the biomass samples adapted to the selection criteria (n.d. not detected). Colour shading indicates the fulfilment of the criteria. Green: fulfilled, yellow: slightly missed, red: clearly missed. Abbreviations: spelt husk (SH), oat husk (OH), digestate (D), foliage (F), rice husk (RH).

Parameter	SH	OH	H	D	F	RH
AC	7.9	5.4	5.6	19.3	10.4	15.5
K ₂ O	6.86	15.0	45.3	8.17	4.38	4.63
MgO	1.11	1.95	3.88	6.96	5.90	0.49
Na ₂ O	n.d.	n.d.	0.39	1.69	0.41	n.d.
P ₂ O ₅	4.23	5.1	7.77	21.6	2.18	0.89
SiO ₂ + Al ₂ O ₃ + Fe ₂ O ₃	85.3	72.7	28.5	17.4	44.7	92.1
SiO ₂	85.0	72.4	27.2	13.4	37.0	91.9
SO ₃	1.44	2.26	5.13	8.62	4.05	0.8
Cl	0.05	0.13	0.81	0.12	0.08	0.12

The biomass husk fuel ashes have a high content of silica. For instance, the silica content of the SH ash reaches 85.0 wt.% db, although it is still lower than the silica content of RH. This high silica content could be an indication that the SH ash is a highly pozzolanic material suitable as an SCM. However, it should be further investigated whether the silica content is in a reactive state. F does not meet all of the criteria (Table 2), e.g., the SO₃ contents are above the limit values. However, it is not considered critical in the role of biomass as an SCM. Thus, SH and F were selected for further analysis, while RH was included as a reference.

3.2. Ash Composition

The visual images of the produced biomass ashes from the ashing process of the selected biomass (SH, F) at different ashing temperatures are shown in Figure 2. For SH, additivated pellets with 1 wt.% kaolin (ASH) were also employed. RH ashes were used as a reference. The white colour in SH, RH, and ASH indicates that these ashes contain a high proportion of silica. In contrast, the F ashes have a slightly brownish colour. For all samples, especially the RH ashes, the higher ashing temperature increases the whiteness of the ashes. The high ashing temperature induces a more complete combustion process and thus removes carbon particles from the produced ash.

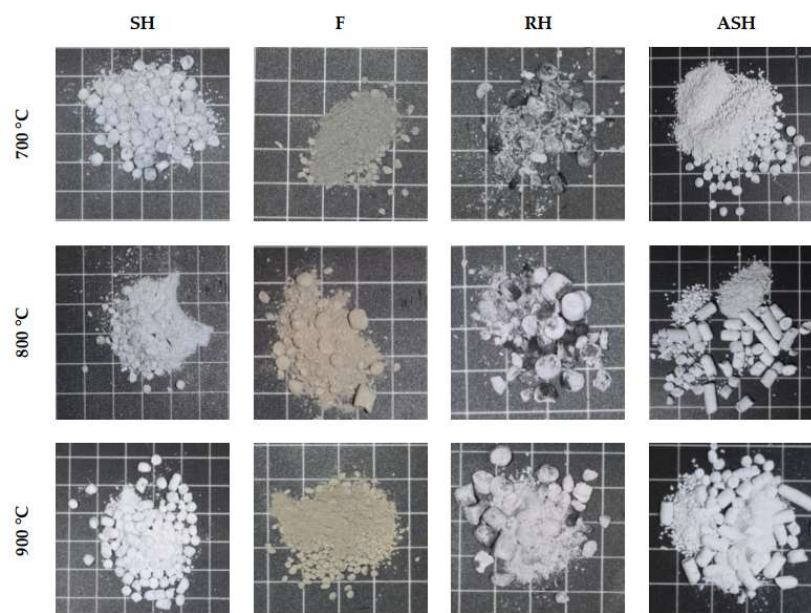


Figure 2. Images of the biomass ash produced at different ashing temperature. Abbreviations: spelt husk (SH), foliage (F), rice husk (RH), additivated spelt husk (ASH).

A significant difference in the granulometry between the F ashes and other ashes can be observed in Figure 2. While the F ashes consist of more pulverised particles, more SH, RH, and ASH ashes retain their pelletised form after the thermal treatment. This effect may be due to the high silica content in SH, RH, and SH ashes. This is probably due to the relatively strong bonds between the silica units [35].

The chemical composition of the ashes is summarised in Table 3. Overall, the difference in the ashing temperature does not significantly affect the chemical composition of the ashes produced. The chemical composition of the ashes also deviates little from the results of the fuel ash analysis in Table 2. This was also highlighted by Zeng et al. for bottom ashes from the combustion of blended biomass pellets in a small-scale combustion appliance [23]. The addition of kaolin to SH increases the content of the pozzolanic oxides (SiO_2 , Al_2O_3 , Fe_2O_3) of ASH, as the major constituents of kaolin are Si and Al, as specified in Table A1. Kaolin in the metastable form of metakaolin has been known for decades to be a highly efficient pozzolanic SCM [54]. The addition of kaolin slightly reduces the silica content of ASH from around 88 wt.% db to around 86 wt.% db because the silica content of kaolin is still much lower than that of SH, which is 52.1 wt.% compared to 88 wt.%. With the addition of 1 wt.% kaolin, the pozzolanic oxide content of ASH is still lower than in the case of RH. From the chemical composition of the ashes, it can be concluded that the SH and ASH ashes are expected to have a pozzolanic higher reactivity than F ashes due to the significantly higher content of the pozzolanic oxide. However, CaO-rich ashes, such as F (see Appendix A Table A2), may exhibit (latent) hydraulic properties.

Table 3. Chemical composition, loss on ignition (LOI), and pH value of the produced biomass ashes adapted to the selection criteria (n.d.: not detected). Abbreviations: spelt husk (SH), foliage (F), rice husk (RH), additivated spelt husk (ASH). The number in the sample name indicates the final ashing temperature.

Ash	K ₂ O	MgO	Na ₂ O	P ₂ O ₅	SiO ₂ + Al ₂ O ₃ + Fe ₂ O ₃	SiO ₂	SO ₃	Cl	LOI	pH
					wt.% db					
SH-700	4.99	1.01	0.04	3.96	88.63	88.42	0.41	0.00	0.28	10.2
SH-800	5.45	1.17	0.05	4.63	86.97	86.75	0.60	0.00	0.17	9.62
SH-900	5.04	1.04	0.06	3.91	88.56	88.35	0.41	0.00	0.14	9.6
F-700	3.83	5.17	0.37	2.48	52.22	45.08	1.23	0.02	0.01	12.9
F-800	3.62	5.12	0.37	2.36	53.02	45.94	1.84	0.00	1.99	13.0
F-900	3.70	5.58	0.39	2.48	47.94	39.92	1.30	0.00	0.78	12.8
RH-700	4.46	0.57	0.11	0.88	92.16	91.80	0.30	0.03	0.64	10
RH-800	4.37	0.52	0.10	0.92	92.27	91.95	0.45	0.00	0.23	9.95
RH-900	4.30	0.56	0.11	0.86	92.45	92.11	0.25	0.00	0.04	9.4
ASH-700	4.80	0.97	0.05	3.58	89.20	85.68	0.28	0.00	0.01	9.1
ASH-800	4.69	0.96	0.05	3.52	89.41	85.90	0.25	n.d.	0.02	9.4
ASH-900	4.78	0.96	0.05	3.50	89.59	86.13	n.d.	n.d.	0.30	9.4

LOI indicates the amount of unburnt carbon in the ash. Although it can also indicate the presence of carbonates and bound water, the major contribution of LOI is mainly residual carbon [55,56]. As shown in Table 3, the LOI of all ashes produced is generally low. The LOI of all samples is less than 2%. The low LOI shows that the biomasses are completely burned during the combustion process. This could be a positive indication, as carbon content in SCMs may cause some disadvantages in the concrete mixture. For instance, the carbon content can reduce the fineness of the ash and, therefore, the reactivity of the cement mixture [55]. Moreover, unburnt carbon has a significant impact on the workability of cement-based materials due to its high surface area.

Table 3 also shows that the pH of all ashes ranges between 9.1 and 12.9. F ashes have the highest pH at more than 12. The ashing temperature does not have a significant impact on the pH of the ashes. The addition of kaolin to SH reduces the pH of ASH ashes. ASH-700 possesses the lowest pH at 9.1. This is due to the addition of acidic compounds in the kaolin, such as SiO₂ and Al₂O₃. A high pH in concrete provides protection against destructive agents that can induce steel corrosion [57]. The pH of the ashes is therefore a positive factor.

3.3. Mineral Phase Characterisation and Prediction

Figure 3 presents the transformation of the mineral phases in ashes as a function of ashing temperatures. XRD analyses indicate that the siliceous biomass ashes produced at 700 °C are characterised by a highly amorphous structure. At 700 °C, the proportion of amorphous structures in SH and RH is 94 wt.% and 96 wt.%, respectively. On the other hand, nearly half of the phases in F transform into crystalline structures at 700 °C. A notable reduction in the amorphous content at higher ashing temperatures can be observed for all non-additive ashes. For instance, the amorphous content decreases from 94 wt.% for SH-700 to 49% for SH-800 and 34% for SH-900, respectively. Crystallisation at higher ashing temperatures has also been reported in previous investigations, although the crystallisation temperature varies depending on the composition of the ash [32,35].

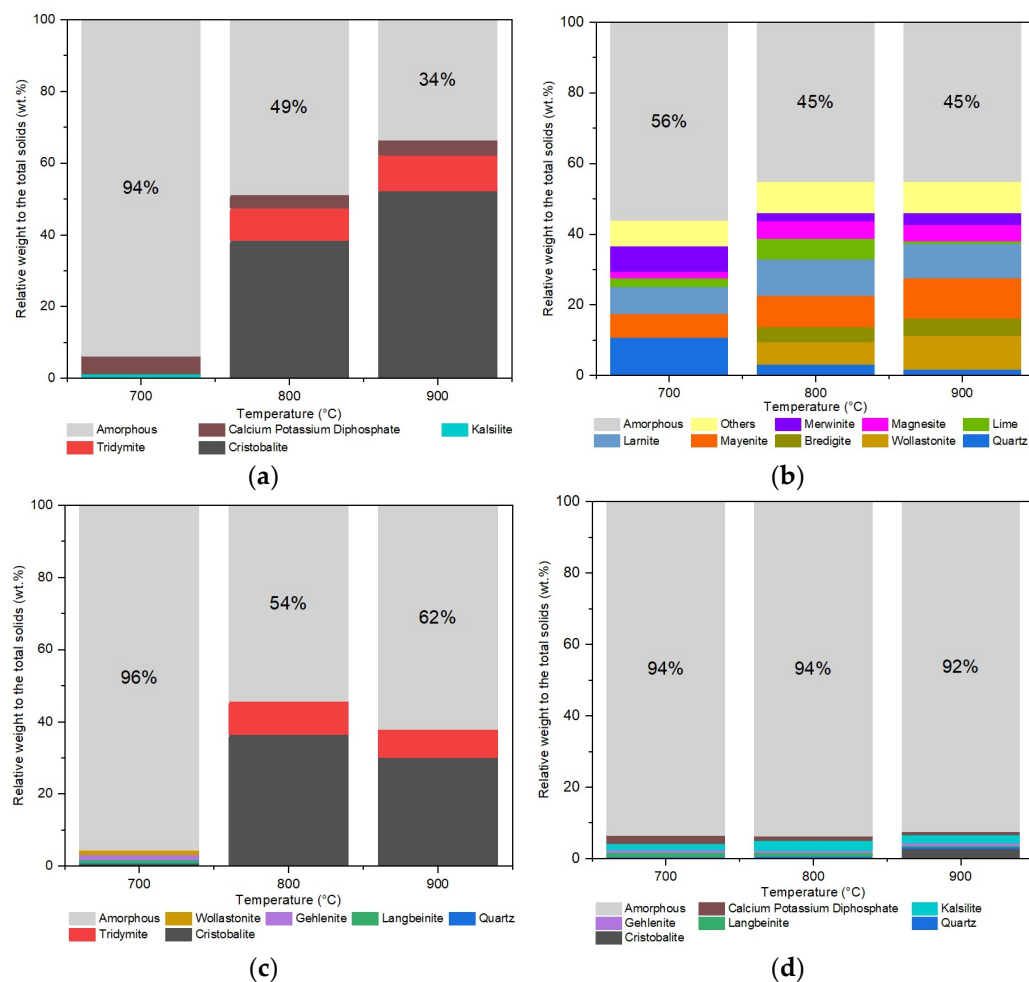


Figure 3. Phase composition of biomass ashes produced at different temperatures detected using XRD: (a) spelt husk (SH), (b) foliage (F), (c) rice husk (RH), (d) additivated spelt husk (ASH). Others in F present the minor phases (<5 wt.%).

As shown in Figure 3, the reduction in amorphous content in SH and RH at higher temperatures is mainly due to the formation of previously reactive amorphous SiO_2 into crystalline mineral phases of simple oxides, such as cristobalite and tridymite. In addition to siliceous crystalline phases, the presence of calcium potassium diphosphate is also detected in SH-800 and SH-900. The phosphorous content in SH ashes is relatively higher than in RH ashes, which, together with the alkali mineral content, contributes to the formation of calcium potassium diphosphate.

As shown in Figure 3c, the amorphous content of RH-900 is 8 wt.% higher than that of RH-800, although the higher ashing temperature should reduce the amorphous content of the ash, as shown clearly in SH. This effect could be due to the inaccuracy of the quantification methods. Some phases sometimes show broadened peaks, making it difficult to distinguish between crystalline and amorphous content, especially in systems with multi-phase and low crystallinity. In principle, the diffraction patterns of RH-800 and RH-900 are very similar, as shown in Figure A1. From a qualitative perspective, the amorphous content of RH-800 and RH-900 should not vary.

Unlike the siliceous ashes, the phase transformation of F ashes is relatively more complex. As shown in Table A2, the major elements of F are CaO (37.6 wt.%) and SiO_2 (37.3 wt.%). Therefore, the mineral phases in F ashes are dominated by the phases in the CaO- SiO_2 phase diagram. At 700 °C, the SiO_2 in the form of quartz accounts for about 10 wt.% of the total phases. The content of quartz decreases at higher temperatures mainly due to the reaction with calcium to form Ca-silicates, like wollastonite (CaSiO_3). Moreover,

a fair amount of mayenite ($\text{Ca}_{12}\text{Al}_{14}\text{O}_{33}$) is present in F ashes, which is formed by the interaction between CaO and Al_2O_3 . The amount of mayenite increases with rising ashing temperatures, reaching more than 11 wt.% at 900 °C. The presence of mayenite in Ca-rich ashes has also been reported in some of the literature [58–60]. The complete results of the XRD analysis of the ashes are presented in Tables A3 and A4.

In contrast to the other ash samples, the reduction of the amorphous content in ASH is not notably detected, as shown in Figure 3. At 900 °C, the proportion of the amorphous phases in ASH still reaches more than 90 wt.%. The addition of kaolin is proven to stabilise the amorphous structure in ASH at high ashing temperatures. The formation of silica-based crystalline structures, like cristobalite and tridymite, which are highly present in SH-800 and SH-900, can be reduced. Kaolinite ($\text{Al}_2\text{Si}_2\text{O}_5(\text{OH})_4$) is the most dominant mineral phase in kaolin [25]. During the thermochemical process, kaolinite releases water and forms meta-kaolinite ($\text{Al}_2\text{O}_3 \cdot 2\text{SiO}_2$), a highly amorphous mixture of alumina and silica. The meta-kaolinite is supposed to bind potassium to form K-Al-silicates, like kalsilite and leucite. As observed in Figure 3, kalsilite is present in ASH ashes in a small amount, which is less than 3%. The potassium content in ASH ashes is much lower than the alumina content. Thus, the absence of potassium might cause the amorphous meta-kaolinite to still be present in ASH ashes.

The slagging tendency of the biomass ashes predicted with the thermodynamic equilibrium calculation is presented in Figure 4. The calculation is based on the chemical composition of the ash samples. As shown in Figure 4, the ashing temperature plays a significant role in the slag formation of SH and RH, because the slag formation increases with the increasing temperature. For instance, the share of slag in SH at 700 °C is around 10%, but it reaches more than 20% at 900 °C. The slag formation at higher temperatures was also indicated by our previous simulation results [35]. This could be due to the melting of the phases with a low melting point, such as K-silicates. On the other hand, the slag formation in F is not detected in the monitored temperature range. The ashes with high CaO content have a higher ash-melting temperature, as reported in [61]. The observation of the slag formation in ASH reveals that the addition of kaolin can inhibit the slagging tendency. At 900 °C, the proportion of slag in ASH remains less than 10%. As mentioned in Section 3.3, the Al in kaolin binds potassium to form K-Al-silicates, such as kalsilite, as presented in Figure 3. Kalsilite is known to have a higher melting temperature than K-silicates. Therefore, the slag formation in ASH can be mitigated.

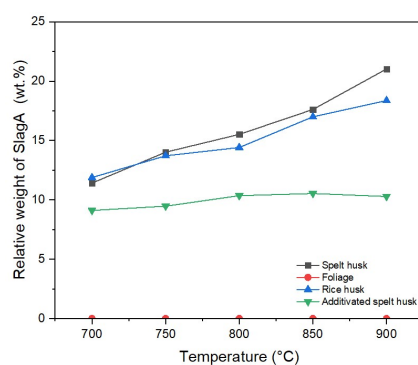


Figure 4. The formation of the solution SlagA with respect to temperature.

The mineral phase transformations calculated using FactSage during the ashing between 700 °C and 900 °C are presented in Figure 5. In general, the simulation using FactSage can predict the presence of similar mineral groups but fails to determine the identical mineral phases detected through the XRD analysis. As shown in Figure 5, SiO_2 -phases are calculated as the most dominant species in SH, RH, and ASH. Nevertheless, the simulation fails to predict the formation of cristobalite, as illustrated in Figure 3. Instead, quartz is formed and completely transformed to tridymite at around 860 °C. Thermodynamically, cristobalite is formed at temperatures above 1400 °C [62]. However, the presence of alkali

metals in biomass ash can significantly reduce the formation temperature of cristobalite. Furthermore, at 700 °C, the proportion of quartz is significantly overestimated because the metastable phases, such as amorphous silica, do not thermodynamically exist [63].

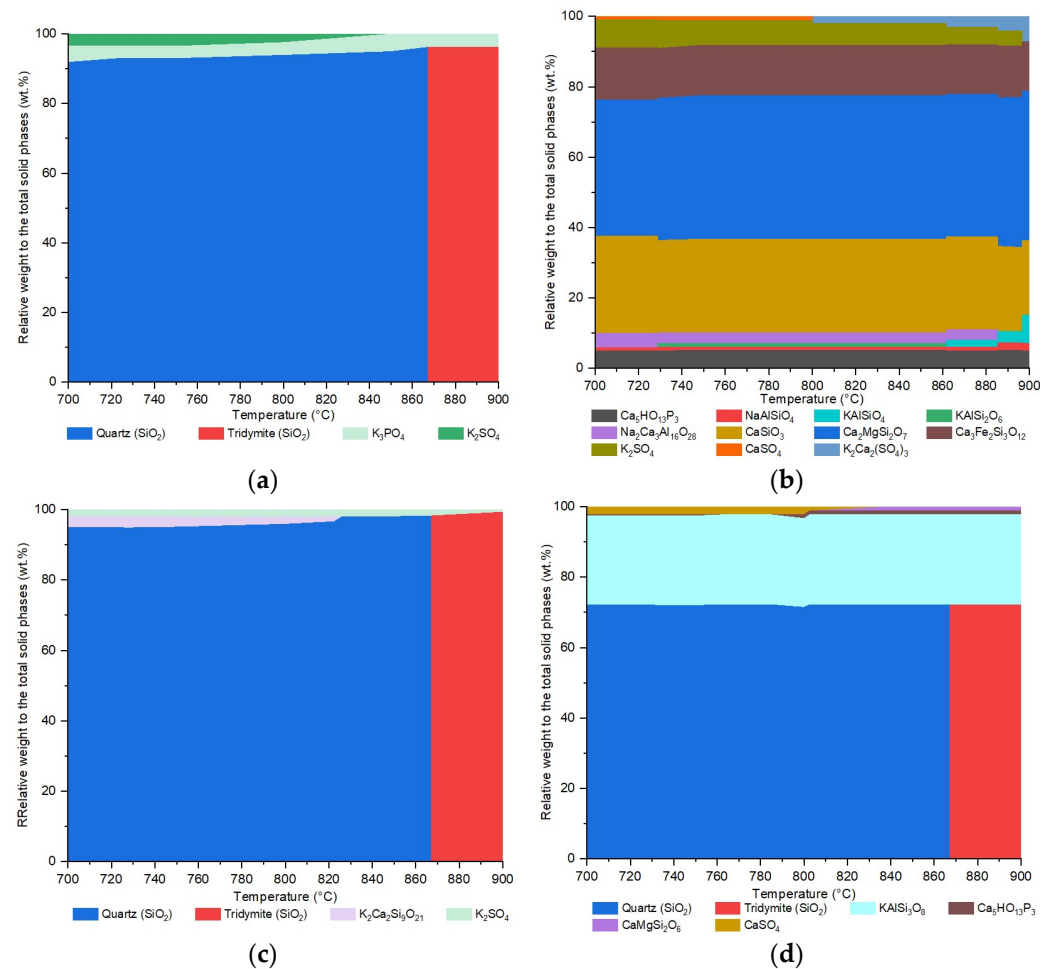


Figure 5. Predicted solid phases of different biomass ashes based on the thermodynamic equilibrium calculation: (a) spelt husk (SH), (b) foliage (F), (c) rice husk (RH), (d) additivated spelt husk (ASH).

The simulation can predict the existence of some similar but not identical mineral phases. For instance, the calculation predicts the minor presence of potassium phosphate (K_3PO_4) in SH instead of calcium potassium diphosphate, as detected through XRD. Moreover, instead of kalsilite, a more stable K-Al-silicate in the form of $KAlSi_3O_8$ is predicted as the second major phase in ASH. The simulation fails to predict silicates, like wollastonite and gehlenite, in RH. Instead, the Ca-silicates are predicted to bind the potassium to form $K_2Ca_2Si_9O_{21}$. For sulphates, instead of gehlenite, the result shows the formation of K_2SO_4 in RH-700.

The phase transformation of F between 700 °C and 900 °C is dominated by the formation of calcium-bearing silicates, such as $CaMgSi_2O_7$, $CaSiO_3$, and $Ca_2Fe_2Si_3O_{12}$, with a total share of around 80%. The group of K-Ca-sulphates is also predicted, which constitutes around 10 wt.% of the total solid mass. The discrepancy between the XRD analysis and the simulation results of F is the failure of the simulation to predict the formation of mayenite, which is one of the most dominant phases in F ashes, according to the XRD results. The simulation predicts only a very small fraction of Ca-aluminate in the form of $Na_2Ca_3Al_{16}O_{28}$. Furthermore, the thermochemical equilibrium calculation fails to predict the formation of simple oxides, such as quartz and lime, as it neglects the kinetic limitations of the process and thus favours the formation of silicates [64].

3.4. Analysis of the Specific Surface Area

In order to analyse the structural characteristics of the ashes, the BET specific surface area (SSA) of the ashes was measured using the gas sorption method. As shown in Figure 6, increasing combustion temperatures result in ashes with lower BET SSA. For instance, the BET of F-900 is 7.5 m²/g, while the BET SSA of F-700 reaches 17.6 m²/g. The decreasing BET SSA of the biomass ashes may be caused by the slag formation process [35,36]. As also shown in the FactSage results in Figure 4, the slag formation tends to increase at higher temperatures, which is in agreement with our previous results [35]. BET SSA is known to have an inverse relationship with the particle size [65,66]. As biomass slag is usually associated with a higher particle size than ash (>3.15 mm) [24,67,68], the BET SSA of biomass slag should be lower.

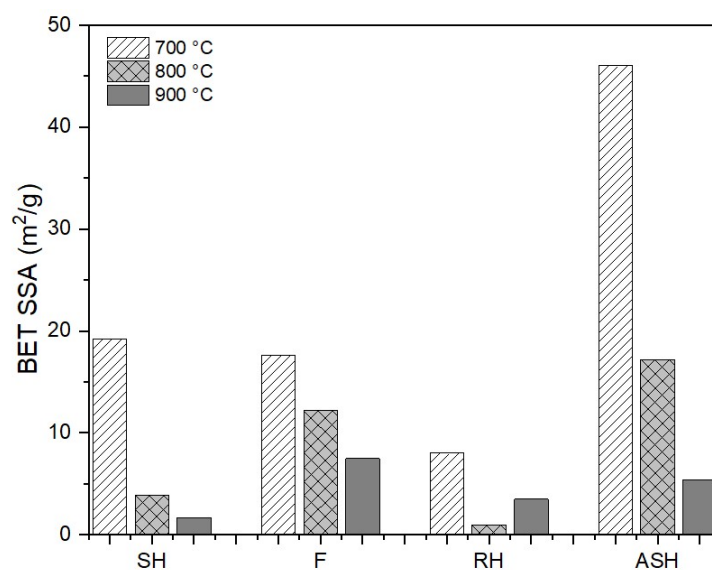


Figure 6. BET SSA of the biomass ashes produced at different ashing temperatures. Abbreviations: spelt husk (SH), foliage (F), rice husk (RH), additivated spelt husk (ASH).

The results of the BET SSA measurement show that RH ashes have a different trend compared to other ashes. While the BET SSA of other ashes decreases with the increasing ashing temperatures, the BET SSA of RH-800 is lower than RH-900. There are some factors that could be the cause of the low BET SSA of RH-800, such as the amorphous content and the particle size. Firstly, the amorphous content of RH ashes shows the same trend as the BET SSA, as shown in Figure 3. At first sight, amorphous content could be directly correlated with BET SSA. However, the results of ASH ashes show that this is not always the case. Secondly, as mentioned earlier, particle size has a direct correlation with BET SSA. RH-800 might have a slightly larger particle size than RH-900. However, as the particle size measurement of ash particles is quite challenging and was not conducted in this study, the actual cause of the low BET SSA value of RH-800 cannot be verified.

The addition of kaolin to the SH significantly improves the BET SSA. At 700 °C, the BET SSA of the SH ash is less than 20 m²/g, while the BET SSA of the ASH ash is more than 46 m²/g. However, the addition of kaolin does not prevent the reduction in the BET SSA in ASH ashes. The BET SSA of ASH ashes significantly decreases to 17.2 m²/g and 5.4 m²/g at 800 °C and 900 °C, respectively. This may be due to the agglomeration of the amorphous structures.

3.5. Evaluation of Pozzolanic Reactivity of the Ashes

The pozzolanic reactivity of the ashes was analysed using the isothermal calorimetry and the bound water measurement. Figure 7 presents the cumulative heat release during the 7-day curing process and the bound water measurement of the cementitious paste made

from biomass ashes. Except for ASH, the heat release measurements were only carried out for the biomass ashes produced at 700 °C. As illustrated in Figure 7, the SH ashes show a comparable reactivity to the RH ashes. SH-700 even has a higher cumulative heat release compared to RH-700. Among the non-additive samples, the highest pozzolanic reactivity was recorded for SH-700 with a bound water of 7.3 g/100 g paste and a cumulative heat release of 385 J/g SCM. The measurement of heat release was conducted to verify the reactivity test according to the bound water measurement.

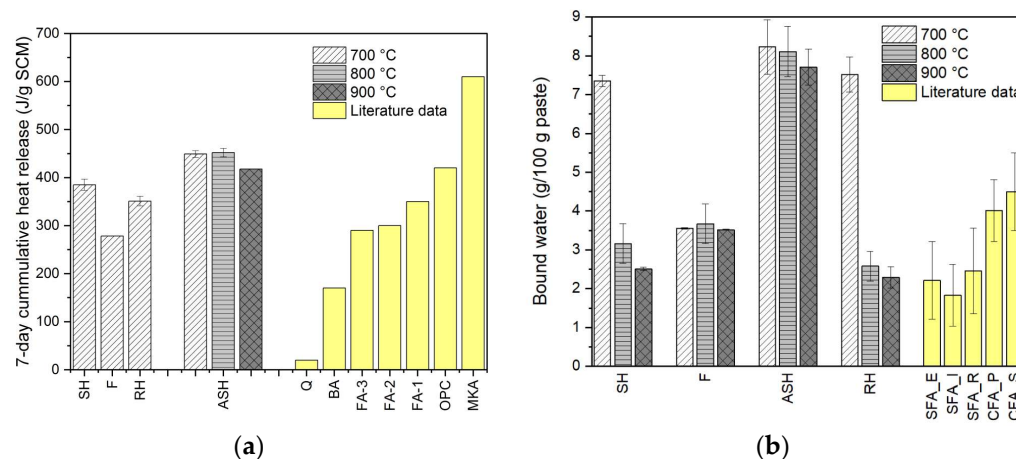


Figure 7. Results of pozzolanic reactivity test: (a) Results of the cumulative heat release generated by different cementitious pastes made from ashes compared to quartz (Q), coal bottom (BA) and fly ash (FA), Portland cement (OPC), and metakaolin (MKA). (b) Results of the bound water measurement of the cementitious paste compared to 3 siliceous fly ash (SFA) and 3 calcareous fly ash (CFA). Literature data were gathered from [47]. Abbreviations: spelt husk (SH), foliage (F), rice husk (RH), additivated spelt husk (ASH).

The bound water of SH decreases significantly at higher ashing temperatures. For instance, the bound water of SH-900 decreases to 2.5 g/100 g paste. This trend is also shown in the RH ashes. The declining reactivity at high ashing temperatures is less pronounced for ASH. This is again due to the stabilised amorphous phase even at high temperatures. Kaolin can also prevent the formation of crystalline structures. In addition, as shown in Figure 7, kaolinite-containing material like metakaolin possesses a very high pozzolanic reactivity. Metakaolin releases about 600 J/g of SCM heat during the seven-day curing process. This could be the reason why the reactivity of ASH is significantly higher than that of SH. Although the addition of kaolin to the biomass pellets was only 1 wt.% of the total mass of the pellets, the proportion of kaolin in ASH increases significantly due to the devolatilization of organic matter during the ashing process. Based on the calculation considering the AC of the SH and the LOI of the kaolin, the proportion of kaolin in the produced ash is about 10 wt.%.

As shown in Figure 8, a close relationship can be observed between the amorphous content and the reactivity of the ash. A highly amorphous structure seems to result in a high reactivity of ash and vice versa. This is mainly because only the active or amorphous fraction participates in the pozzolanic reaction [69]. Thus, the amorphousness of SCMs is an important factor in determining reactivity.

On the other hand, the relationship between the BET SSA and the reactivity of the ash is more complicated. A higher specific surface area provides more sites for the hydration reaction to happen simultaneously. Nevertheless, if the whole grains dissolve over time, the total reaction measured will not be affected. Thus, the BET SSA of the biomass-based SCM only affects the rate of reaction and has a limited effect on the total reactivity measured after seven days.

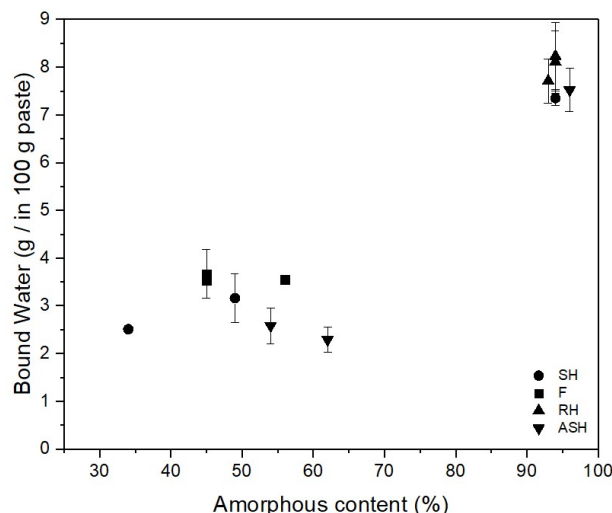


Figure 8. Correlation between the amorphous content and the bound water measurement of the ashes. Abbreviations: spelt husk (SH), foliage (F), rice husk (RH), additivated spelt husk (ASH).

4. Conclusions and Future Perspectives

The following conclusions can be drawn from this study:

- Spelt husk and foliage are promising biomasses due to their high AC, low content of critical ash-forming elements, and high content of pozzolanic oxides. The other studied biomasses appear less suitable due to their fuel ash composition. For instance, hay and oat husk contain a high amount of potassium, while the phosphorus content of digestate is very high.
- The BET SSA, amorphous content, and reactivity of the ashes tend to decrease with increasing ashing temperature. This is mainly due to the formation of crystalline structures at higher temperatures.
- The results of thermodynamic equilibrium calculation can qualitatively predict the mineral phases present in the ash but fail to recognise identical species that are detected through XRD analysis. The calculation is limited by the neglect of process kinetics and the mass–heat transfer phenomena.
- The addition of kaolin to biomass through, in this case, spelt husk, increases the reactivity of the ash. Moreover, it can also reduce the effect of increasing ashing temperature on the reactivity of the ash by stabilising the amorphous structure and preventing the formation of crystalline-like structures.
- In terms of bound water measurement, the additivated spelt husk ash shows a higher reactivity compared to other coal fly ashes. The heat release measurement even proves that the reactivity of the additivated spelt husk ash produced in the monitored temperature range is comparable to that of Portland cement.

The findings of this study are important for evaluating the potential of spelt husk ash as an SCM. The evaluation of the application of biomass ash as SCMs in real cement mixture is currently underway. Further evaluation of this study will be based on the validation of the characteristic and homogeneity of the produced ash with regards to its use as SCM in real-scale combustion tests, including the influence of different combustion technologies (fixed bed, fluidised bed, etc.) and the impact of combustion conditions. In addition, a deeper investigation on the influence of the particle size of the ash and other additives on the performance of ash as an SCM is also interesting.

Author Contributions: Conceptualisation, H.B.D., T.Z. and S.O.; methodology, H.B.D., S.O., D.K., R.D.P. and T.Z.; software, R.D.P.; validation, R.D.P.; formal analysis, R.D.P.; investigation, R.D.P., D.K. and H.B.D.; resources, T.Z.; data curation, R.D.P.; writing—original draft preparation, R.D.P.; writing—review and editing, S.O., H.B.D., T.Z. and A.V.; visualisation, R.D.P., D.K. and H.B.D.; supervision, T.Z., H.B.D. and A.V.; project administration, T.Z. and S.O.; funding acquisition, T.Z. and A.V. All authors have read and agreed to the published version of the manuscript.

Funding: This work is funded by the Federal Ministry for Economy Affairs and Climate Action of Germany through the ‘BioBeton’ Project under grant agreement number KK5045102KI0.

Data Availability Statement: Data are contained within this article.

Acknowledgments: The support of our industry partners Treffler Maschinenbau GmbH & Co. KG and TBS Transportbeton im Osthafen Frankfurt GmbH & Co. KG is greatly acknowledged.

Conflicts of Interest: The authors declare no conflicts of interest.

Appendix A

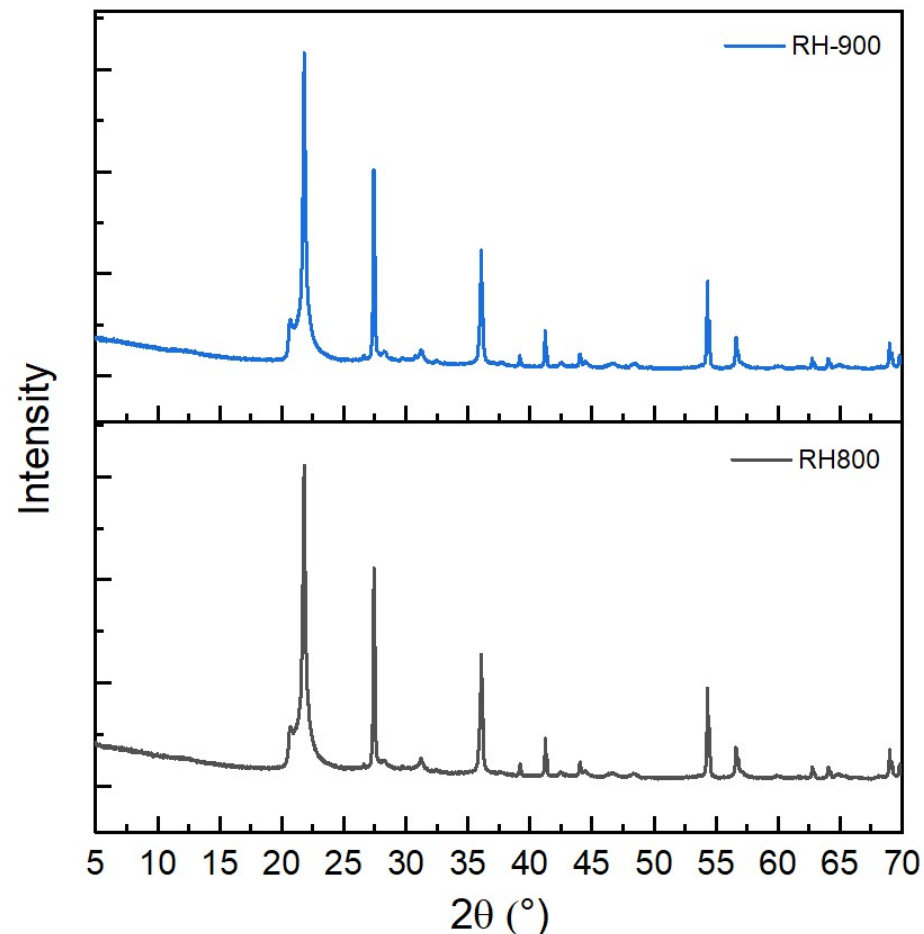


Figure A1. XRD diffractogram of rice husk ash produced at 900 °C (top) and 800 °C (bottom).

Table A1. Chemical composition of the kaolin from the supplier.

Parameter	Unit	Value
LOI	wt.% db	11.8
Al ₂ O ₃	wt.% db	34.1
CaO	wt.% db	0.1
Fe ₂ O ₃	wt.% db	0.60
K ₂ O	wt.% db	0.60
MgO	wt.% db	0.1
Na ₂ O	wt.% db	0.00
SiO ₂	wt.% db	52.1
TiO ₂	wt.% db	0.6

Table A2. Complete chemical element compositions of the analysed fuel.

Parameter	Unit	SH	OH	H	D	F	RH	ASH
C *	wt.% db	43.50	45.40	45.90	41.20	46.90	41.40	44.30
H *	wt.% db	5.46	5.42	5.84	4.59	5.15	4.90	4.92
N *	wt.% db	0.47	0.35	1.10	2.41	0.91	0.45	0.38
S *	wt.% db	0.05	0.05	0.10	0.62	0.15	0.05	0.05
Cl *	wt.% db	0.05	0.13	0.81	0.12	0.08	0.12	0.05
O *	wt.% db	50.47	48.65	46.25	51.06	46.81	53.08	50.30
Fuel ash composition								
Al ₂ O ₃ *	wt.% db	0.18	0.15	0.85	1.15	3.19	0.16	4.17
BaO	wt.% db	0.01	0.01	0.03	0.02	0.04	n.d.	0.01
CaO *	wt.% db	1.03	2.96	8.63	34.62	37.69	0.89	1.10
CdO	wt.% db	0.00	0.00	n.d.	0.00	0.00	0.00	n.d.
Cr ₂ O ₃	wt.% db	0.01	0.01	0.01	0.02	0.03	0.01	0.01
CuO	wt.% db	0.00	0.00	n.d.	0.05	0.01	0.00	0.00
Fe ₂ O ₃ *	wt.% db	0.09	0.14	0.44	2.83	4.45	0.08	0.41
K ₂ O *	wt.% db	6.86	14.95	45.30	8.17	4.38	4.63	5.41
MgO *	wt.% db	1.11	1.95	3.88	6.96	5.90	0.49	1.13
MnO *	wt.% db	0.03	0.06	0.18	0.36	0.22	0.17	0.04
Na ₂ O *	wt.% db	0.00	0.00	0.39	1.69	0.41	0.00	0.05
NiO	wt.% db	0.00	0.01	n.d.	0.01	0.01	0.00	0.00
P ₂ O ₅ *	wt.% db	4.23	5.10	7.77	21.58	2.18	0.89	1.46
PbO	wt.% db	n.d.						
SiO ₂ *	wt.% db	84.98	72.37	27.21	13.43	37.03	91.86	84.68
TiO ₂	wt.% db	0.00	0.00	0.08	0.09	0.25	0.00	0.14
ZnO	wt.% db	0.01	0.03	0.05	0.33	0.08	0.01	0.01

* inputs to FactSage simulation.

Table A3. Complete mineral phases transformation in SH, RH, and ASH ashes detected using XRD.

Phase	°C	SH			RH			ASH		
		700	800	900	700	800	900	700	800	900
Amorphous	wt.%	93.8	48.8	33.6	96.5	54.3	62.2	93.5	93.7	92.5
Cristobalite	SiO ₂ wt.%	n.d.	38.5	52.3	0.6	36.4	30.1	n.d.	0.1	2.8
Tridymite	SiO ₂ wt.%	n.d.	9	9.8	n.d.	9.3	7.7	n.d.	n.d.	n.d.
Quartz	SiO ₂ wt.%	n.d.	n.d.	n.d.	0.3	n.d.	n.d.	0.5	0.6	0.5
Langbeinite	Mg ₂ K ₂ (SO ₄) ₃ wt.%	n.d.	n.d.	n.d.	0.9	n.d.	n.d.	1.1	0.9	0.3
Gehlenite	Ca ₂ Al[AlSiO ₇] wt.%	n.d.	n.d.	n.d.	1.4	n.d.	n.d.	0.8	0.7	0.8
Wollastonite	CaSiO ₃ wt.%	n.d.	n.d.	n.d.	1.2	n.d.	n.d.	n.d.	n.d.	n.d.
Kalsilite	KAlSiO ₄ wt.%	1.3	n.d.	n.d.	n.d.	n.d.	n.d.	1.8	2.7	2.3
Calcium Potassium Diphosphate	CaKOP ₄ wt.%	4.9	3.7	4.3	n.d.	n.d.	n.d.	2.3	1.3	0.9

Table A4. Complete mineral phases transformation in F ashes detected using XRD.

Phase	°C	F			
		700	800	900	
Amorphous	wt. %	56.1	45.1	45	
Quartz	SiO ₂	wt. %	10.7	3.2	1.8
Aphthitalite	(K,Na) ₃ Na(SO ₄) ₂	wt. %	n.d.	1.6	1.6
Wollastonite	CaSiO ₃	wt. %	n.d.	6.4	9.4
Gehlenite	Ca ₂ Al	wt. %	n.d.	3.8	3.2
Bredigite	Ca ₇ MgSi ₄ O ₁₆	wt. %	n.d.	4.2	5
Mayenite	Ca ₁₂ O ₇ Al ₂ O ₃	wt. %	6.9	8.9	11.4
Larnite	Ca ₂ SiO ₄	wt. %	7.5	10.3	9.6
Lime	CaO	wt. %	2.6	5.7	0.7
Calcite	CaCO ₃	wt. %	1.8	0.6	0.5
Anhydrite	CaSO ₄	wt. %	0.3	1.7	2.4
Anorthoclase	(Na,K)AlSi ₃ O ₈	wt. %	2.7	n.d.	n.d.
Barite	BaSO ₄	wt. %	0.7	0.8	0.7
Fluorite	CaF ₂	wt. %	1.8	0.3	0.5
Magnesite	MgCO ₃	wt. %	1.7	5	4.6
Merwinite	Ca ₃ Mg[SiO ₄] ₂	wt. %	7.2	2.4	3.4

References

- Scrivener, K.L.; John, V.M.; Gartner, E.M. Eco-efficient cements: Potential economically viable solutions for a low-CO₂ cement-based materials industry. *Cem. Concr. Res.* **2018**, *114*, 2–26. [[CrossRef](#)]
- Pamenter, S.; Myers, R.J. Decarbonizing the cementitious materials cycle: A whole-systems review of measures to decarbonize the cement supply chain in the UK and European contexts. *J. Ind. Ecol.* **2021**, *25*, 359–376. [[CrossRef](#)]
- Habert, G.; Miller, S.A.; John, V.M.; Provis, J.L.; Favier, A.; Horvath, A.; Scrivener, K.L. Environmental impacts and decarbonization strategies in the cement and concrete industries. *Nat. Rev. Earth Environ.* **2020**, *1*, 559–573. [[CrossRef](#)]
- Miller, S.A.; Habert, G.; Myers, R.J.; Harvey, J.T. Achieving net zero greenhouse gas emissions in the cement industry via value chain mitigation strategies. *One Earth* **2021**, *4*, 1398–1411. [[CrossRef](#)]
- United Nations/Framework Convention on Climate Change. Paris Agreement. In Proceedings of the UN Climate Change Conference, Paris, France, 12 December 2015.
- Juenger, M.C.; Snellings, R.; Bernal, S.A. Supplementary cementitious materials: New sources, characterization, and performance insights. *Cem. Concr. Res.* **2019**, *122*, 257–273. [[CrossRef](#)]
- Lothenbach, B.; Scrivener, K.; Hooton, R.D. Supplementary cementitious materials. *Cem. Concr. Res.* **2011**, *41*, 1244–1256. [[CrossRef](#)]
- European Commission; Joint Research Centre. *Brief on Biomass for Energy in the European Union*; Publications Office of the EU: Luxembourg, 2019.
- Cabrera, M.; Díaz-López, J.L.; Agrela, F.; Rosales, J. Eco-Efficient Cement-Based Materials Using Biomass Bottom Ash: A Review. *Appl. Sci.* **2020**, *10*, 8026. [[CrossRef](#)]
- Obernberger, I.; Supancic, K. Possibilities of Ash Utilisation from Biomass Combustion Plants. In Proceedings of the 17th European Biomass Conference & Exhibition, Hamburg, Germany, 29 June–3 July 2009; ETA-Florence Renewable Energies: Florence, Italy, 2009.
- Jhatial, A.A.; Nováková, I.; Gjerløw, E. A Review on Emerging Cementitious Materials, Reactivity Evaluation and Treatment Methods. *Buildings* **2023**, *13*, 526. [[CrossRef](#)]
- Kusuma, R.T.; Hiremath, R.B.; Rajesh, P.; Kumar, B.; Renukappa, S. Sustainable transition towards biomass-based cement industry: A review. *Renew. Sustain. Energy Rev.* **2022**, *163*, 112503. [[CrossRef](#)]
- Chowdhury, S.; Maniar, A.; Suganya, O.M. Strength development in concrete with wood ash blended cement and use of soft computing models to predict strength parameters. *J. Adv. Res.* **2015**, *6*, 907–913. [[CrossRef](#)]
- Fořt, J.; Šál, J.; Žák, J.; Černý, R. Assessment of Wood-Based Fly Ash as Alternative Cement Replacement. *Sustainability* **2020**, *12*, 9580. [[CrossRef](#)]
- Fořt, J.; Šál, J.; Ševčík, R.; Doleželová, M.; Keppert, M.; Jerman, M.; Záleská, M.; Stehel, V.; Černý, R. Biomass fly ash as an alternative to coal fly ash in blended cements: Functional aspects. *Constr. Build. Mater.* **2021**, *271*, 121544. [[CrossRef](#)]
- Jaworska, B.; Stańczak, D.; Tarańska, J.; Jaworski, J. The Influence of Cement Substitution by Biomass Fly Ash on the Polymer-Cement Composites Properties. *Materials* **2021**, *14*, 3079. [[CrossRef](#)] [[PubMed](#)]
- Berra, M.; Mangialardi, T.; Paolini, A.E. Reuse of woody biomass fly ash in cement-based materials. *Constr. Build. Mater.* **2015**, *76*, 286–296. [[CrossRef](#)]
- Ottosen, L.M.; Hansen, E.Ø.; Jensen, P.E.; Kirkelund, G.M.; Golterman, P. Wood ash used as partly sand and/or cement replacement in mortar. *Int. J. Sustain. Dev. Plan.* **2016**, *11*, 781–791. [[CrossRef](#)]

19. Feng, Q.; Yamamichi, H.; Shoya, M.; Sugita, S. Study on the pozzolanic properties of rice husk ash by hydrochloric acid pretreatment. *Cem. Concr. Res.* **2004**, *34*, 521–526. [CrossRef]
20. Wu, K.; Han, H.; Rößler, C.; Xu, L.; Ludwig, H.M. Rice husk ash as supplementary cementitious material for calcium aluminate cement—Effects on strength and hydration. *Constr. Build. Mater.* **2021**, *302*, 124198. [CrossRef]
21. Hu, L.; He, Z.; Zhang, S. Sustainable use of rice husk ash in cement-based materials: Environmental evaluation and performance improvement. *J. Clean. Prod.* **2020**, *264*, 121744. [CrossRef]
22. Pollex, A.; Zeng, T.; Khalsa, J.; Erler, U.; Schmersahl, R.; Schön, C.; Kuptz, D.; Lenz, V.; Nelles, M. Content of potassium and other aerosol forming elements in commercially available wood pellet batches. *Fuel* **2018**, *232*, 384–394. [CrossRef]
23. Zeng, T.; Pollex, A.; Weller, N.; Lenz, V.; Nelles, M. Blended biomass pellets as fuel for small scale combustion appliances: Effect of blending on slag formation in the bottom ash and pre-evaluation options. *Fuel* **2018**, *212*, 108–116. [CrossRef]
24. Mack, R.; Kuptz, D.; Schön, C.; Hartmann, H. Combustion behavior and slagging tendencies of kaolin additivated agricultural pellets and of wood-straw pellet blends in a small-scale boiler. *Biomass Bioenergy* **2019**, *125*, 50–62. [CrossRef]
25. Boström, D.; Grimm, A.; Boman, C.; Björnbom, E.; Öhman, M. Influence of Kaolin and Calcite Additives on Ash Transformations in Small-Scale Combustion of Oat. *Energy Fuels* **2009**, *23*, 5184–5190. [CrossRef]
26. Xiong, S.; Burvall, J.; Öberg, H.; Kalen, G.; Thyrel, M.; Öhman, M.; Boström, D. Slagging Characteristics during Combustion of Corn Stovers with and without Kaolin and Calcite. *Energy Fuels* **2008**, *22*, 3465–3470. [CrossRef]
27. Wang, L.; Hustad, J.E.; Skreiberg, Ø.; Skjevrak, G.; Grønli, M. A Critical Review on Additives to Reduce Ash Related Operation Problems in Biomass Combustion Applications. *Energy Procedia* **2012**, *20*, 20–29. [CrossRef]
28. Shun, D.; Choi, Y.; Jun, H.; Lee, D.-H.; Shin, J.-S.; Han, K.H.; Lee, S.Y.; Bae, D.H. Effect of kaolinite on control of hard deposit formation and alteration of fine particles in a commercial circulating fluidized bed boiler burning solid refuse fuel. *Powder Technol.* **2021**, *389*, 549–560. [CrossRef]
29. Eurostat. Crop Production in National Humidity (from 2000 Onwards). Available online: https://ec.europa.eu/eurostat/databrowser/view/APRO_CPNH1/default/table?lang=en (accessed on 1 June 2023).
30. Ganesan, K.; Rajagopal, K.; Thangavel, K. Rice husk ash blended cement: Assessment of optimal level of replacement for strength and permeability properties of concrete. *Constr. Build. Mater.* **2008**, *22*, 1675–1683. [CrossRef]
31. Thomas, B.S. Green concrete partially comprised of rice husk ash as a supplementary cementitious material—A comprehensive review. *Renew. Sustain. Energy Rev.* **2018**, *82*, 3913–3923. [CrossRef]
32. Beidaghy Dizaji, H.; Zeng, T.; Hartmann, I.; Enke, D.; Schliermann, T.; Lenz, V.; Bidabadi, M. Generation of High Quality Biogenic Silica by Combustion of Rice Husk and Rice Straw Combined with Pre- and Post-Treatment Strategies—A Review. *Appl. Sci.* **2019**, *9*, 1083. [CrossRef]
33. Schliermann, T.; Hartmann, I.; Beidaghy Dizaji, H.; Zeng, T.; Schneider, D.; Wassersleben, S.; Enke, D.; Jobst, T.; Lange, A.; Roelofs, F.; et al. High Quality Biogenic Silica from Combined Energetic and Material Utilization of Agricultural Residues. In Proceedings of the 7th International Symposium on Energy from Biomass and Waste, Prague, Czech Republic, 2–5 July 2018.
34. Dizaji, H.B.; Zeng, T.; Enke, D. Mitigation of Ash-Melting Behavior during Combustion of Silica-Rich Biomass Assortments to Enhance Porosity of Biogenic Silica. In Proceedings of the 29th European Biomass Conference and Exhibition (EUBCE 2021), Marseille, France, 26–29 April 2021; ETA-Florence Renewable Energies: Firenze, Italy, 2021.
35. Beidaghy Dizaji, H.; Zeng, T.; Hölzig, H.; Bauer, J.; Klöß, G.; Enke, D. Ash transformation mechanism during combustion of rice husk and rice straw. *Fuel* **2022**, *307*, 121768. [CrossRef]
36. Beidaghy Dizaji, H.; Zeng, T.; Enke, D. New fuel indexes to predict ash behavior for biogenic silica production. *Fuel* **2022**, *310*, 122345. [CrossRef]
37. DIN EN ISO 18122:2016-03; Deutsches Institut für Normung e.V. Biogene Festbrennstoffe-Bestimmung des Aschegehaltes. Beuth Verlag GmbH: Berlin, Germany, 2015.
38. DIN EN ISO 16967:2015-07; Deutsches Institut für Normung e.V. Biogene Festbrennstoffe-Bestimmung von Hauptelementen-Al, Ca, Fe, Mg, P, K, Si, Na und Ti. Beuth Verlag GmbH: Berlin, Germany, 2015.
39. DIN EN 15935:2021-10; Deutsches Institut für Normung e.V. Boden, Abfall, behandelter Bioabfall und Schlamm-Bestimmung des Glühverlusts. Beuth Verlag GmbH: Berlin, Germany, 2021.
40. Thommes, M.; Kaneko, K.; Neimark, A.V.; Olivier, J.P.; Rodriguez-Reinoso, F.; Rouquerol, J.; Sing, K.S. Physisorption of gases, with special reference to the evaluation of surface area and pore size distribution (IUPAC Technical Report). *Pure Appl. Chem.* **2015**, *87*, 1051–1069. [CrossRef]
41. Webb, P.A.; Orr, C. *Analytical Methods in Fine Particle Technology*, 1st, ed.; Micromeritics Instrument Corp: Norcross, GA, USA, 1997; ISBN 096567830X.
42. Schneider, D.; Wassersleben, S.; Weiß, M.; Denecke, R.; Stark, A.; Enke, D. A Generalized Procedure for the Production of High-Grade, Porous Biogenic Silica. *Waste Biomass Valor.* **2020**, *11*, 1–15. [CrossRef]
43. Zarehassangheshlaghi, A.; Beidaghy Dizaji, H.; Zeng, T.; Huth, P.; Ruf, T.; Denecke, R.; Enke, D. Behavior of Metal Impurities on Surface and Bulk of Biogenic Silica from Rice Husk Combustion and the Impact on Ash-Melting Tendency. *ACS Sustain. Chem. Eng.* **2020**, *8*, 10369–10379. [CrossRef]
44. ASTM D4972-18; Standard Test Methods for pH of Soils. ASTM International: West Conshohocken, PA, USA, 2019.
45. ASTM C1897-20; Standard Test Methods for Measuring the Reactivity of Supplementary Cementitious Materials by Isothermal Calorimetry and Bound Water Measurements. ASTM International: West Conshohocken, PA, USA, 2020.

46. Avet, F.; Snellings, R.; Alujas Diaz, A.; Ben Haha, M.; Scrivener, K. Development of a new rapid, relevant and reliable (R3) test method to evaluate the pozzolanic reactivity of calcined kaolinitic clays. *Cem. Concr. Res.* **2016**, *85*, 1–11. [[CrossRef](#)]
47. Li, X.; Snellings, R.; Antoni, M.; Alderete, N.M.; Ben Haha, M.; Bishnoi, S.; Cizer, Ö.; Cyr, M.; de Weerd, K.; Dhandapani, Y.; et al. Reactivity tests for supplementary cementitious materials: RILEM TC 267-TRM phase 1. *Mater. Struct.* **2018**, *51*, 151. [[CrossRef](#)]
48. Lindberg, D.; Backman, R.; Chartrand, P.; Hupa, M. Towards a comprehensive thermodynamic database for ash-forming elements in biomass and waste combustion—Current situation and future developments. *Fuel Process. Technol.* **2013**, *105*, 129–141. [[CrossRef](#)]
49. Atallah, E.; Defoort, F.; Pisch, A.; Dupont, C. Thermodynamic equilibrium approach to predict the inorganic interactions of ash from biomass and their mixtures: A critical assessment. *Fuel Process. Technol.* **2022**, *235*, 107369. [[CrossRef](#)]
50. *DIN EN 450-1:2012*; Deutsches Institut für Normung e.V. Flugasche für Beton-Teil 1: Definition, Anforderungen und Konformitätskriterien. Beuth Verlag GmbH: Berlin, Germany, 2012.
51. Berenguer, R.; Lima, N.; Pinto, L.; Monteiro, E.; Povoas, Y.; Oliveira, R.; Lima, N. Cement-based materials: Pozzolanic activities of mineral additions are compromised by the presence of reactive oxides. *J. Build. Eng.* **2021**, *41*, 102358. [[CrossRef](#)]
52. Boström, D.; Skoglund, N.; Grimm, A.; Boman, C.; Öhman, M.; Broström, M.; Backman, R. Ash Transformation Chemistry during Combustion of Biomass. *Energy Fuels* **2012**, *26*, 85–93. [[CrossRef](#)]
53. Pang, X.; Cuello Jimenez, W.; Singh, J. Measuring and modeling cement hydration kinetics at variable temperature conditions. *Constr. Build. Mater.* **2020**, *262*, 120788. [[CrossRef](#)]
54. Sabir, B.; Wild, S.; Bai, J. Metakaolin and calcined clays as pozzolans for concrete: A review. *Cem. Concr. Compos.* **2001**, *23*, 441–454. [[CrossRef](#)]
55. Chen, H.-J.; Shih, N.-H.; Wu, C.-H.; Lin, S.-K. Effects of the Loss on Ignition of Fly Ash on the Properties of High-Volume Fly Ash Concrete. *Sustainability* **2019**, *11*, 2704. [[CrossRef](#)]
56. Dodson, V.H. *Concrete Admixtures*; Springer: Boston, MA, USA, 1990; ISBN 978-1-4757-4845-1.
57. Sumra, Y.; Payam, S.; Zainah, I. The pH of Cement-based Materials: A Review. *J. Wuhan Univ. Technol.-Mat. Sci. Edit.* **2020**, *35*, 908–924. [[CrossRef](#)]
58. Houda Hamsi, N.E.; Nabih, K.; Barbach, R. The benefic effect of Moroccan oil shale’s ash on blended cement (CMII). *MATEC Web Conf.* **2018**, *149*, 1023. [[CrossRef](#)]
59. Qiao, X.C.; Tyrer, M.; Poon, C.S.; Cheeseman, C.R. Characterization of alkali-activated thermally treated incinerator bottom ash. *Waste Manag.* **2008**, *28*, 1955–1962. [[CrossRef](#)] [[PubMed](#)]
60. Zhao, Z.; Wang, R.; Wu, J.; Yin, Q.; Wang, C. Bottom ash characteristics and pollutant emission during the co-combustion of pulverized coal with high mass-percentage sewage sludge. *Energy* **2019**, *171*, 809–818. [[CrossRef](#)]
61. Lachman, J.; Baláš, M.; Lisý, M.; Lisá, H.; Milčák, P.; Elbl, P. An overview of slagging and fouling indicators and their applicability to biomass fuels. *Fuel Process. Technol.* **2021**, *217*, 106804. [[CrossRef](#)]
62. Driscoll, K.E.; Guthrie, G.D. Crystalline Silica and Silicosis. In *Comprehensive Toxicology*; Elsevier: Amsterdam, The Netherlands, 2010; pp. 331–350. ISBN 9780080468846.
63. Baccarin, L.; Bielefeldt, W.V.; Bragança, S.R. Evaluation of thermodynamic simulation (FactSage) for the interpretation of the presence of phases and the firing behavior of triaxial ceramics. *Ceram. Int.* **2021**, *47*, 21522–21529. [[CrossRef](#)]
64. Reinmöller, M.; Klinger, M.; Schreiner, M.; Gutte, H. Relationship between ash fusion temperatures of ashes from hard coal, brown coal, and biomass and mineral phases under different atmospheres: A combined FactSage™ computational and network theoretical approach. *Fuel* **2015**, *151*, 118–123. [[CrossRef](#)]
65. Dubois, I.E.; Holgersson, S.; Allard, S.; Malmström, M.E. Dependency of BET surface area on particle size for some granitic minerals. *Proc. Radiochem.* **2011**, *1*, 75–82. [[CrossRef](#)]
66. Rahman, I.A.; Vejayakumaran, P.; Sipaut, C.S.; Ismail, J.; Chee, C.K. Size-dependent physicochemical and optical properties of silica nanoparticles. *Mater. Chem. Phys.* **2009**, *114*, 328–332. [[CrossRef](#)]
67. Schön, C.; Feldmeier, S.; Hartmann, H.; Schwabl, M.; Dahl, J.; Rathbauer, J.; Vega-Nieva, D.J.; Boman, C.; Öhman, M.; Burval, J. New Experimental Evaluation Strategies Regarding Slag Prediction of Solid Biofuels in Pellet Boilers. *Energy Fuels* **2019**, *33*, 11985–11995. [[CrossRef](#)]
68. Wang, X.; Zhu, Y.; Hu, Z.; Zhang, L.; Yang, S.; Ruan, R.; Bai, S.; Tan, H. Characteristics of ash and slag from four biomass-fired power plants: Ash/slag ratio, unburned carbon, leaching of major and trace elements. *Energy Convers. Manag.* **2020**, *214*, 112897. [[CrossRef](#)]
69. Walker, R.; Pavia, S. Physical properties and reactivity of pozzolans, and their influence on the properties of lime–pozzolan pastes. *Mater. Struct.* **2011**, *44*, 1139–1150. [[CrossRef](#)]

Disclaimer/Publisher’s Note: The statements, opinions and data contained in all publications are solely those of the individual author(s) and contributor(s) and not of MDPI and/or the editor(s). MDPI and/or the editor(s) disclaim responsibility for any injury to people or property resulting from any ideas, methods, instructions or products referred to in the content.